Thin Solid Films 698 (2020) 137845

Contents lists available at ScienceDirect

Thin Solid Films

journal homepage: www.elsevier.com/locate/tsf

Tin oxide nanosheet thin film with bridge type structure for gas sensing

Pil Gyu Choi[a], Naoto Shirahata[b,c,d], Yoshitake Masuda[a,*]

[a] National Institute of Advanced Industrial Science and Technology (AIST), 2266-98 Anagahora, Shimoshidami, Moriyama, Nagoya, 463-8560, Japan
[b] International Center for Materials Nanoarchitectonics (WPI-MANA), National Institute for Materials Science (NIMS), 1-1, Namiki, Tsukuba, 305-0044, Japan
[c] Department of Physics, Chuo University, 1-13-27 Kasuga, Bunkyo, Tokyo 112-8551, Japan
[d] Graduate School of Chemical Sciences and Engineering, Hokkaido University, Sapporo 060-0814, Japan

ARTICLE INFO

Keywords:
Tin oxide
Nanosheet
Thin film
Bridge type structure
Gas sensor

ABSTRACT

A bridge type structure of the SnO_2 nanosheet thin film was formed on the Pt interdigitated-electrodes printed SiO_2 substrate via a simple synthesis process. The SnO_2 nanosheet has ca. 150 nm of flat plane and extremely thin thickness. In addition, the thin film between Pt interdigitated-electrodes was floated from the substrate. It was found that the sensor signal response considerably increased by using the SnO_2 nanosheet thin film with bridge type structure as compared to the SnO_2 nanosheet with normal structure, especially for extremely low concentration of nonanal gas which is biomarker of lung cancer. The higher sensing response was attributed to introduction of space under thin film which acts as reaction rooms and provide the plenty of time to stay for the reaction.

Introduction

Human life expectancy has been increasing at a rapid rate. With the increase of the life expectancy, early diagnosis of disease and stress management are essential to healthy life. Human produce specific chemical substances when they feel stressed, age, or caught the disease [1–5]. Although diagnosis of disease and stress management is easily realized by sensing the chemical substances, it is difficult to detect the chemical substances due to those extremely low concentrations. Therefore, it is necessary to develop a highly sensitive gas sensor.

It is well known that tin oxide (SnO_2) exhibits superior sensing response for inflammable gases and volatile organic compounds [6–10], since SnO_2 possess n-type semiconducting properties attributed to adequate band gap energy [11–13]. SnO_2 is therefore one of the first considered and is still the most frequently used material in gas sensor fields. Moreover, because of the characteristic properties of nanomaterials, many nanostructured SnO_2 was released with development of nanotechnology [9, 14–17]. amongst the various structure, nanosheet structure is considered one of the ideal structures for sensors because well-defined nanosheet possesses a high surface-to-volume ratio as well as specific exposed crystal facets.

In our previous studies, an easy process for synthesis of a SnO_2 nanosheet thin film at moderate temperature without any additives was developed and the SnO_2 nanosheet thin film directly synthesized on the sensor chip by the process [18]. In addition, since the synthesized SnO_2 nanosheet exposed specific surface crystal facet, the SnO_2 nanosheet exhibited fast response and recovery speed as compared to SnO_2 nanoparticle [19], and higher selectivity for alkene gases than alkane gases [20].

In the present study, for effective detection of the chemical substances, SnO_2 with the nanosheet structure was adopted. Furthermore, it was found that a bridge type structure was formed on the SiO_2 substrate after the SnO_2 nanosheet thin film synthesis and expected increase of sensing properties as compared to the normal structure. Therefore, the sensing properties of the SnO_2 nanosheet thin film with bride type structure were evaluated with hydrogen gas (H_2), methane gas (CH_4), as well as nonanal ($C_9H_{18}O$) gas which is biomarker of lung cancer [3, 21]. Additionally, effects of the bridge type structure of thin film for gas sensing were investigated as compared to the normal thin film structure.

* Corresponding author.
E-mail address: masuda-y@aist.go.jp (Y. Masuda).

https://doi.org/10.1016/j.tsf.2020.137845
Received 8 October 2019; Received in revised form 16 January 2020; Accepted 6 February 2020
Available online 07 February 2020
0040-6090/

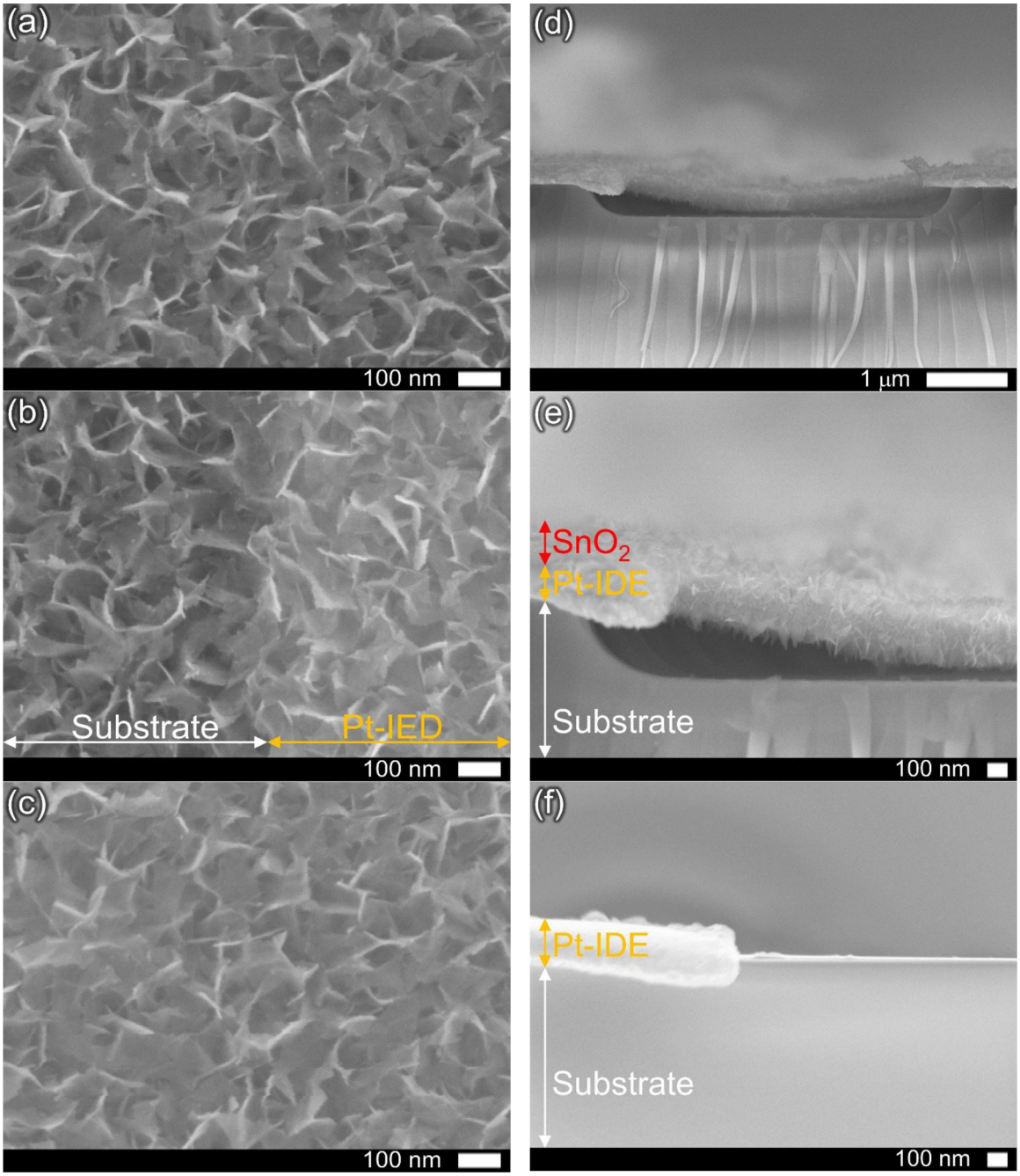

Fig. 1. FE-SEM images of (a) BS on the SiO_2 substrate, (b), BS on the SiO_2 substrate and Pt-IED, (c) BS on Pt-IED, (d) cross-section of BS between Pt-IEDs, (e) cross-section of BS on the SiO_2 substrate and Pt-IED, and (f) before the BS fabrication.

Experimental procedure

A SnO_2 nanosheet thin film with bridge type structure (hereinafter referred to as "BS") was synthesized using SnF_2 (Wako Pure Chemical Industries, Ltd., 90.0% pure) via an aqueous solution process on Pt interdigitated-electrodes (Pt-IEDs) printed SiO_2 substrate (G-IDEPT, Drop Sens). The surface of the substrate was cleaned using a vacuum ultraviolet light (PL16-10 low-pressure mercury lamp, air flow, 100 V, 200 W, SEN Lights Co.) for 20 min. to ensure the effective nucleation and growth of the SnO_2 nanosheet thin film [22]. The surface of the substrate, excluding Pt-IEDs printed area, was taped to control synthesis area. Then, the substrate was set in a polypropylene vessel and placed against a wall with Pt-IEDs facing down to prevent a pile-up of the precipitates. The vessel pre-heated at 90 °C using a drying oven (DKN402, Yamato Scientific Co., Ltd.,). 90 °C of SnF_2 aqueous solution was added to the vessel, where concentration of SnF_2 solution was

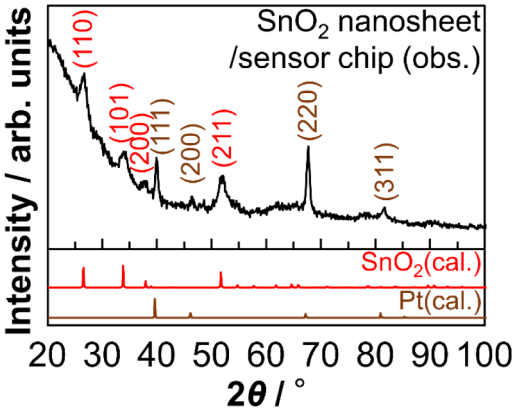

Fig. 2. GIXD pattern of BS.

0.028 M. Subsequently, the temperature of the vessel was maintained at 90 °C for 6 h using drying oven to synthesize BS. After then, the sample was rinsed under running water and was dried at room temperature, and the tape was removed. For comparison, the normal structure of the SnO_2 nanosheet thin film (hereinafter referred to as "NS") was fabricated on Pt-IEDs printed Al_2O_3 substrate via the identical process, where a combo-type electrode with 0.05 mm of gap, 0.05 mm of width, and 0.5 mm of length was printed on 650 × 2250 mm^2.

The surface morphology of the obtained SnO_2 nanosheet thin film was observed using a field emission-scanning electron microscope (10 kV) (FE-SEM; JSM-6335FM, JEOL Ltd.). High resolution-transmission electron microscopy (200 kV), energy dispersive X-ray spectroscopy, and a fast Fourier transform (HR-TEM, EDS, and FFT; Tecnai Osiris, FEL) were conducted to observe detailed structure. The TEM sample was prepared using a focused ion beam. Grazing incidence X-ray diffraction (GIXD; SmartLab, Rigaku) patterns of the SnO_2 nanosheet thin film was obtained using the parallel beam geometry with Cu Kα radiation (40 kV, 30 mA) in the 2θ ranges 20–100°

To assess the gas sensing properties, the sample was placed in a quartz chamber, which was set in a furnace. After setting, the temperature was increased to the operating temperature of 300 °C and stabilization was carried out at the operating temperature for 3 h under a flow of compressed air. The concentration of hydrogen (H_2) or methane (CH_4) gas was controlled by mixing pure gas (GL Science Inc., 99.9% pure). Nonanal ($C_9H_{18}O$) gas was generated using nonanal solution (Tokyo Chemicals Industry Co., Ltd., ≥ 95.0% pure) via a gas generator (PD-1B, GASTEC Co.). The total gas flow rate into the chamber was maintained at 100 cm^3 min^{-1}. The electrical resistance of the SnO_2 nanosheet thin film between Pt-IEDs was measured under compressed air and the target gas. The electrical resistance was recorded using a digital multimeter/switch system (Model 2700, Keithley, Instruments Inc.). The sensor signal response relative to the target gas was defined as $(R_a\text{-}R_g)/R_g$, where R_a and R_g were the electrical resistances under air and the target, respectively.

Results and discussion

The formed SnO_2 nanosheet thin film was observed (Fig. 1). The SnO_2 nanosheet has ca. 150 nm of flat plane and extremely thin thickness. The SnO_2 nanosheets were not overlapped and they were orientated such that the edge of one SnO_2 nanosheet was in contact with the flat surface of another. the SnO_2 nanosheet thin film was floated from the substrate to form a bridge structure (Fig. 1(d) and (e)). The Pt-IDE was played a role of a pier and the SnO_2 nanosheet thin film was connecting the Pt-IDEs. The SnO_2 nanosheet was grown not only in upward direction but also on the back site of the thin film. The thickness of BS was therefore identical to two times of the size of the SnO_2 nanosheet, thus that was ca. 300 nm. It was observed that surface of the substrate was flat and was placed in similar highest before the synthesis of the SnO_2 nanosheet thin film (Fig. 1(f)). After synthesis of the SnO_2 nanosheet thin film, the surface of the SiO_2 substrate was eroded. It was considered that BS was form by eroding of the SiO_2 substrate. The formation mechanism is presented below equations [23].

$$SnF_2 + (OH)^- \rightarrow SnF(OH) + F^- \quad (1\text{–}1)$$

$$SnF(OH) + (OH)^- \rightarrow Sn(OH)_2 + F^- \quad (1\text{–}2)$$

$$Sn(OH)_2 \rightarrow SnO + H_2O \quad (1\text{–}3)$$

$$Sn(OH)_2 \rightarrow SnO + H_2 \quad (1\text{–}4)$$

$$SnO + H_2O \rightarrow SnO_2 + H_2 \quad (1\text{–}5)$$

The SnF_2 precursor dissociated with their ions, when they dissolved in distilled water. After then, the ionized Sn^{2+} combined with $(OH)^-$ in distilled water and formed $Sn(OH)_2$. Finally, SnO_2 was obtained by the dehydration and condensation reaction of $Sn(OH)_2$. The F^- ion was generated in the SnO_2 formation process and etched the SiO_2 substrate. As a result, a gap was created between the SnO_2 nanosheet thin film and the SiO_2 substrate. Then, the solution was permeated to the created gap. Therefore, The SnO_2 was grown not only in upward direction but also on the back site of the thin film with extending the gap. Finally, the bridge type structure of SnO_2 nanosheet thin film as shown in Fig. 1 was obtained.

The X-ray diffraction was performed in order to analyse the crystal structure of BS. GIXD pattern of BS is shown in Fig. 2. The peaks at 2θ = 26.7, 33.9, 37.6 and 52.1° were indexed to (110), (101), (200), and (211) for the tetragonal cassiterite structure of SnO_2 with the space group $P4_2/mnm$, respectively. The peaks at 2θ = 39.9, 46.3, 67.7, and 81.7° were assigned to (111), (200), (220), and (311) for Pt which were attributed to Pt-IDs, respectively. This result indicated that BS was synthesized.

TEM and HR-TEM was conducted for detailed morphology analysis and Fig. 3 shows the cress-section TEM image of BS. The nanosheet structure was clearly observed and the nanosheets was stood perpendicular to Pt-IED. Moreover, the SnO_2 nanosheet was grown on the back site of the thin film from end of Pt-IED (yellow arrow in Fig. 3(a)). Additionally, small size of SnO_2 was observed inside the SnO_2 nanosheet thin film (yellow arrow in Fig. 3(b)) and has nanosheet structure (Fig. 3(c)). The thickness of the SnO_2 nanosheet was ca. 3 nm (Fig. 3(d)) and arrangement of atoms was observed, indicating high degree of crystallinity (Fig. 3(e)). A layer distance of d = 0.264 nm was measured at the atomic arrangement shown on the cross-section of the SnO_2 nanosheet, which corresponds to d space of the SnO_2 (101) face (Fig. 3(f)).

High-angle annular dark field (HAADF) and TEM-EDS of BS were shown in Fig. 4. There was a clear distinction amongst the SiO_2 substrate, Pt-IED, and the SnO_2 nanosheet thin film, respectively (Fig. 4(a)). Sn, Si, Pt were detected in BS, the substrate, and Pt-IED, respectively. O was detected both in the thin film with bride type structure and in the substrate.

NS, not bridge type structure, was prepared by using the Pt-IEDs printed Al_2O_3 substrate for comparison. Since the concentration of the

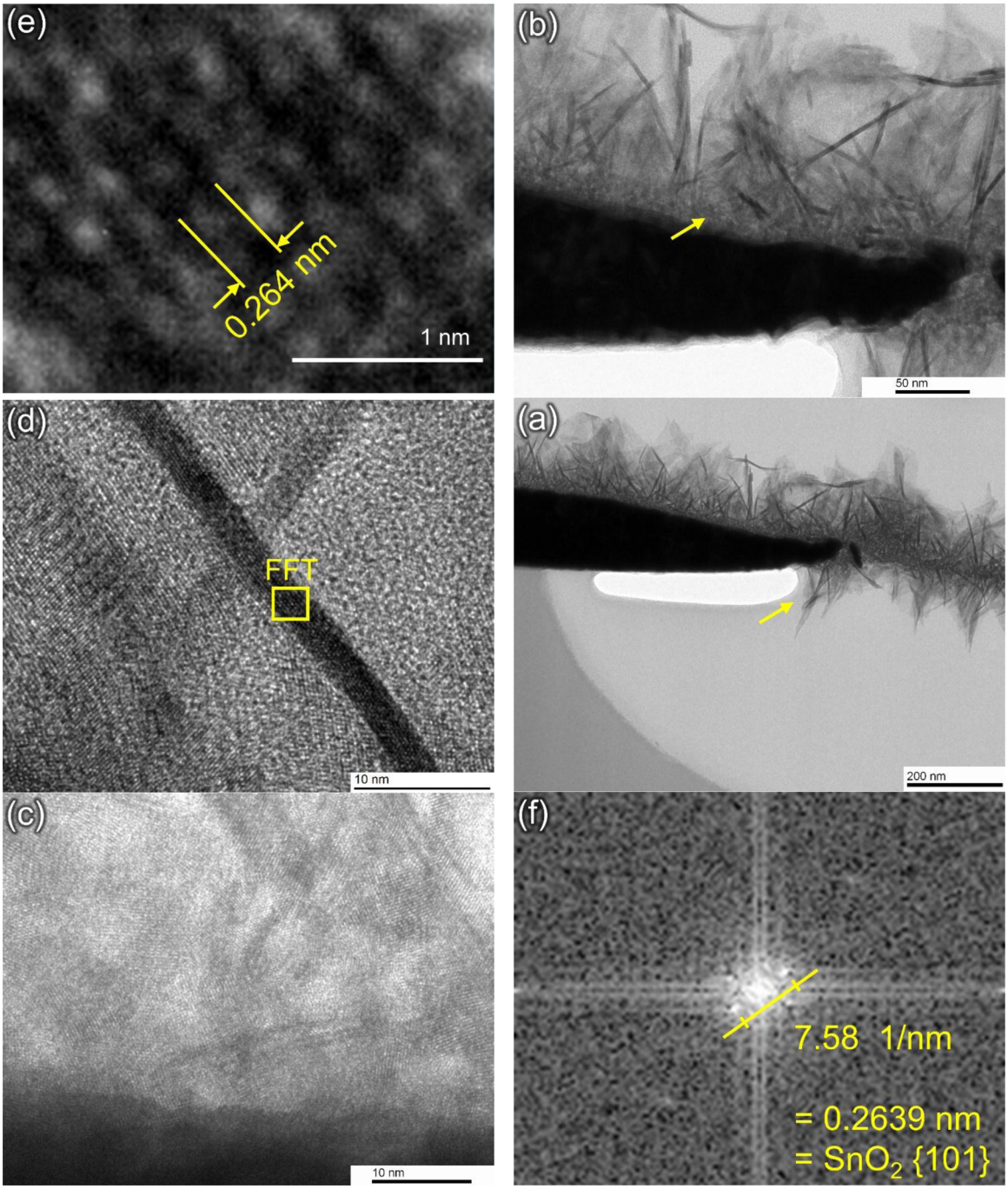

Fig. 3. TEM, HR-TEM, and FFT pattern images of (a) BS on the SiO_2 substrate and Pt-IED, (b) BS on the edge of Pt-IED, (c)BS on Pt-IED, (d) cross-section of the nanosheet, (e) atomic arrangements on the cross-section of nanosheet, and (f) FFT pattern on cross-section of nanosheet. .

generated F^- ion from the 0.028 M of SnF_2 aqueous solution was enough to etch the SiO_2 substrate, BS was obtained on the SiO_2 substrate. In the case of the Al_2O_3 substrate, it is difficult to etch as compared to the SiO_2 substrate using F^- ion, thus the etching reaction was difficult to progress in the condition. Therefore, NS was obtained on the Pt-IEDs printed Al_2O_3 substrate. NS has the identical crystal structure and sheet size as compared to BS. The formed SnO_2 nanosheet thin film on the Pt-IEDs printed Al_2O_3 substrate was observed (Fig. 5). The SnO_2 nanosheet has ideal structure to BS, that is ca. 150 nm of flat plane and extremely thin thickness. The SnO_2 nanosheets stood perpendicular to the substrate and were connected with one another in such a manner that the edge of the one SnO_2 nanosheet connected the flat surface of the others. The NS was formed to single layer fallowing surface of the Al_2O_3 grain and Pt-IEDs (Fig. 5(d) and (f)). The thickness of NS was therefore ca. 150 nm.

The nanosheet structure stood perpendicular to the Al_2O_3 substrate

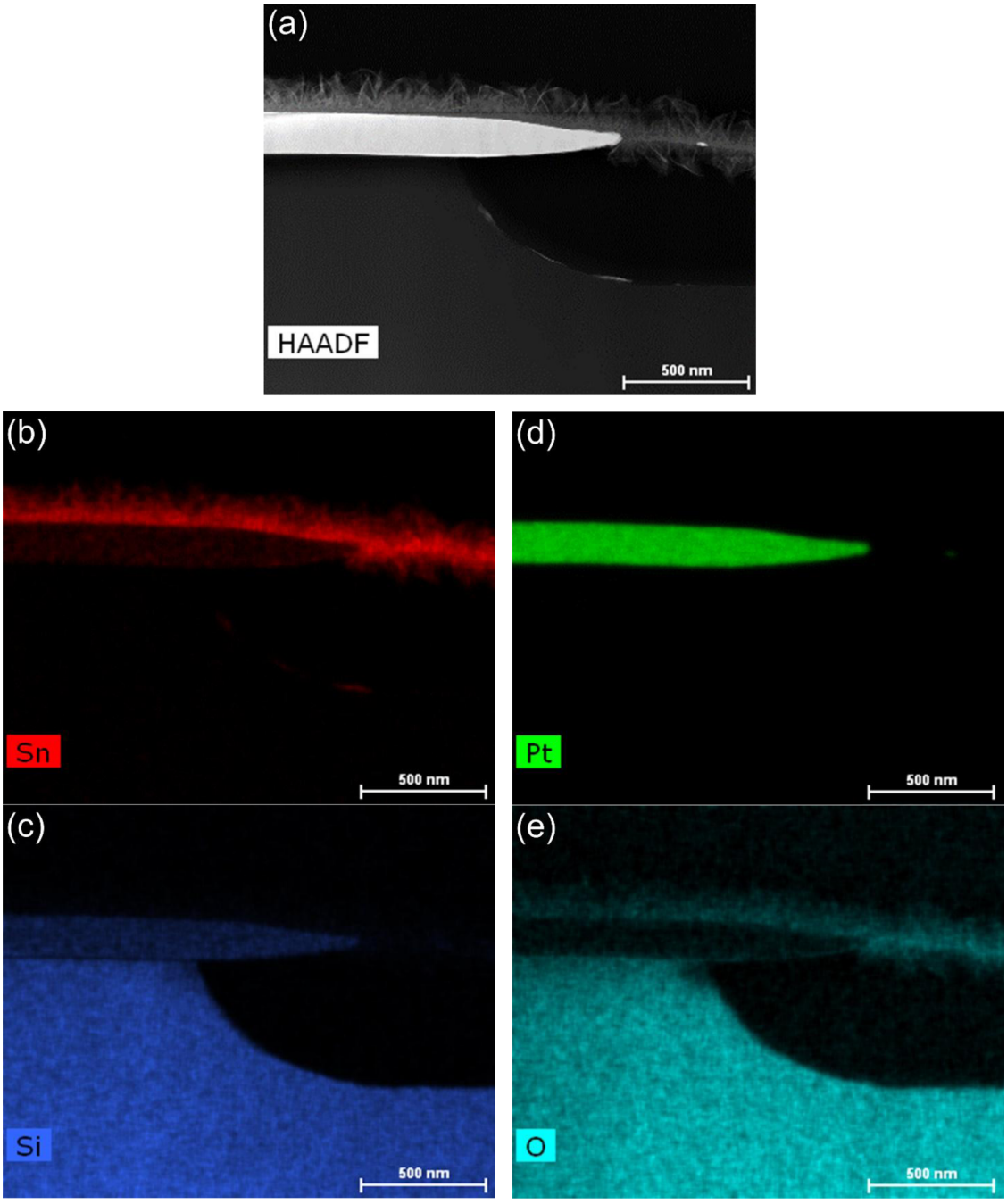

Fig. 4. HAADF and TEM-EDS images of BS; (a) HAADF, (b) Sn, (c) Si, (d) Pt, and (e) O.

and Pt-IED was clearly observed (Fig. 6(a) and (b)). The thickness of the SnO_2 nanosheet was ca. 5 nm (Fig. 6(c)) and arrangement of atoms was observed, indicating high degree of crystallinity (Fig. 6(d)). A layer distance of $d = 0.264$ nm was measured at the atomic arrangement shown on the cross-section of the SnO_2 nanosheet, which corresponds to d space of the SnO_2 (101) face (Fig. 6(e)).

High-angle annular dark field (HAADF) and TEM-EDS of NS were shown in Fig. 7. There was a clear distinction amongst the Al_2O_3 substrate, Pt-IED, and the SnO_2 nanosheet thin film, respectively (Fig. 7(a)). Sn, Al, Pt were detected in NS, the substrate, and Pt-IED, respectively. O was detected both in the thin film with bride type structure and in the substrate.

BS and NS were adopted for a gas sensor and the sensor signal response are shown in Fig. 8. Both of BS and NS exhibited a degree of sensitivity that was typical of an n-type semiconductor gas sensor. The electrical resistance was decreased when the sensor was exposed to the target gas. The electrical resistance returned to the initial level when the target gas replaced with air. The electrical resistance dynamic range

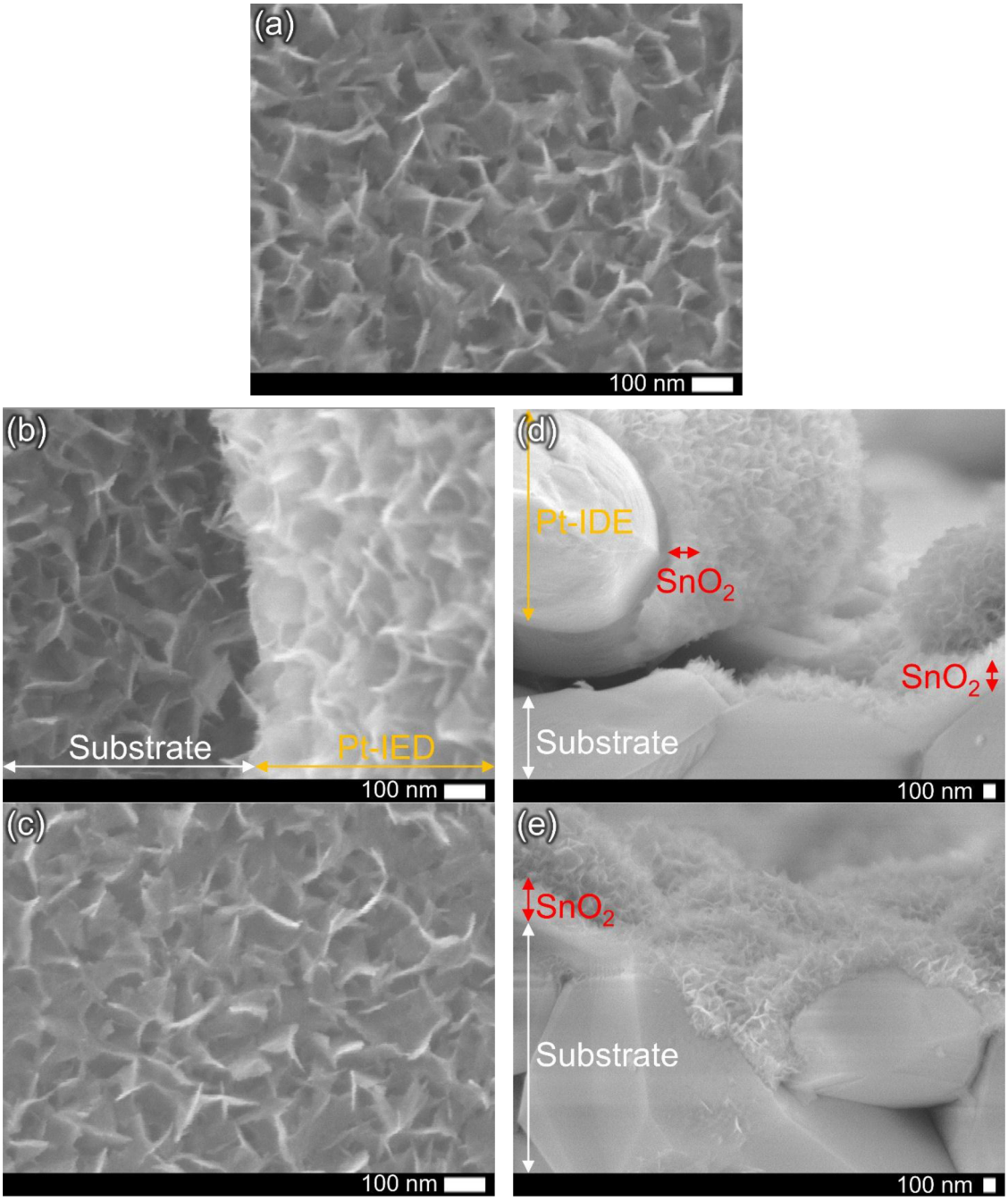

Fig. 5. FE-SEM images of (a) NS on the Al_2O_3 substrate. (b) SN on the Al_2O_3 substrate and Pt-IED, (c) NS on Pt-IED, (d) cross-section of NS on the Al_2O_3 substrate and Pt-IED, and (e) cross-section of NS on the Al_2O_3 substrate.

for the gases increased in order of 500 ppm of CH_4 < 0.85 ppm of $C_9H_{18}O$ < 500 ppm of H_2 in the case of BS (Fig. 9(a)). NS exhibited the electrical resistance variation for H_2 gas and extremely low electrical resistance variation for CH_4 and $C_9H_{18}O$ gases. The electrical resistance dynamic range for the gases increased in order of 0.85 ppm of $C_9H_{18}O$ < 500 ppm of CH_4 < 500 ppm of H_2 (Fig. 9(b)).

The sensor signal response ratio of BS to NS is shown in Fig. 10. The value of the response ratio was greater than 1, indicating that BS has the superior sensing response than NS. Especially, the response ration for $C_9H_{18}O$ gas was significantly high, even though the gas concentration of $C_9H_{18}O$ was considerably lower than H_2 and CH_4 gases. Thus, the results indicated that the gas sensing selectivity to $C_9H_{18}O$ gas can be improved by using BS.

In general, the sensing reaction mechanism of SnO_2 can be described by ionosorption model [24]; When oxygen is adsorbed on the surface, electrons in the conduction band are trapped by the adsorbed

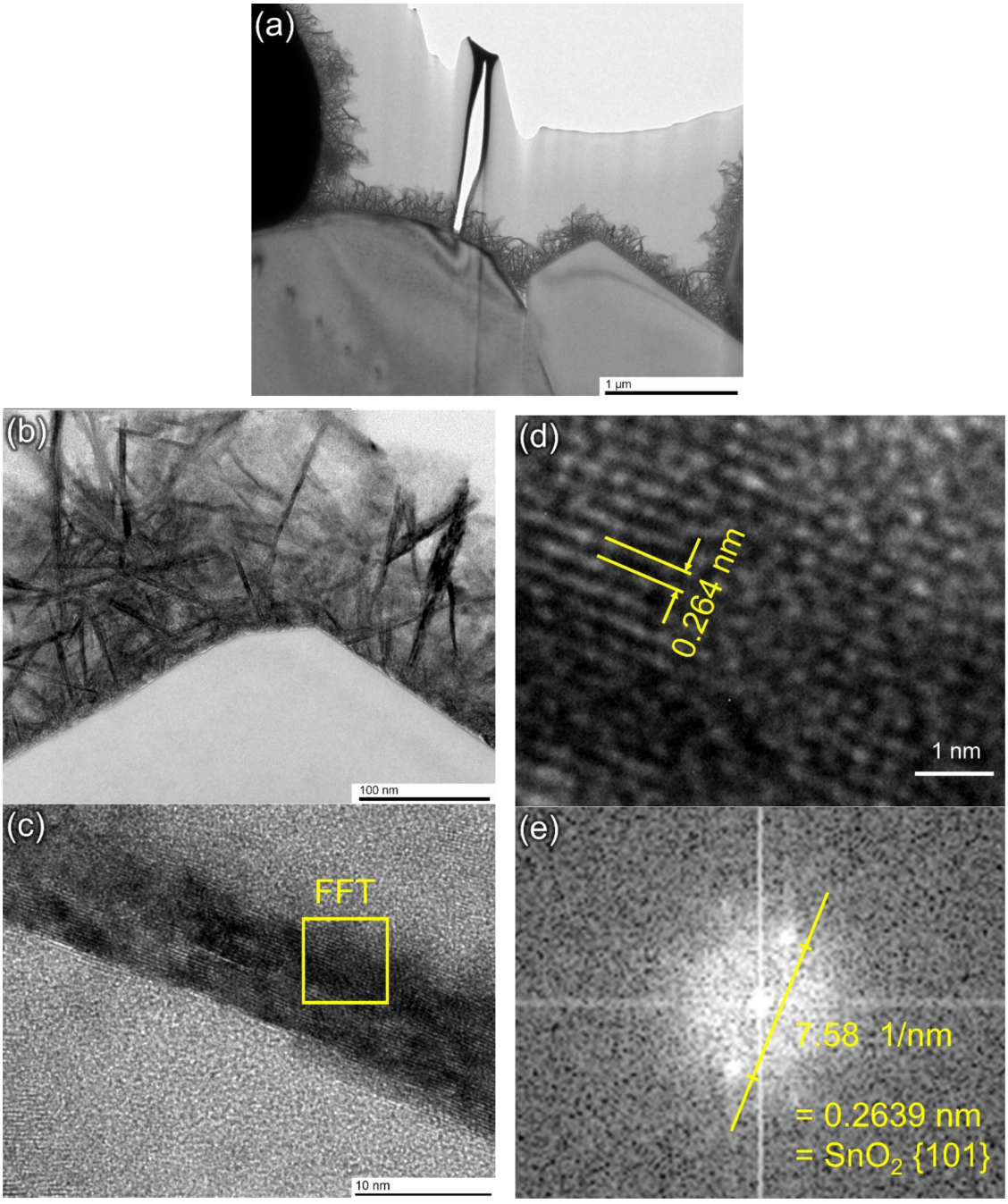

Fig. 6. TEM, HR-TEM, and FFT pattern images of (a) NS on the Al_2O_3 substrate and Pt-IED, (b) NS on the Al_2O_3 substrate, (c) cross-section of nanosheet, (d) atomic arrangements on cross-section of nanosheet, and (e) FFT patterns on cross-section of nanosheet.

oxygen. Therefore, an electron-depleted layer is extended on the surface of SnO_2. In this state, when the target gas is introduced, the gas molecules react with the adsorbed oxygen. By this reaction, electrons return to the conduction band, thereby thinning the electron-depleted layer and decreasing the electrical resistance of SnO_2. In the case of the SnO_2 nanosheet, reaction described by an oxygen-vacancy model dominantly occur [24–26], due to its specific exposed crystal facet which is (101) SnO_2 crystal facet [20, 21]; When the target gas introduced, the target gas molecules reacted with lattice oxygen in the surface of the SnO_2 nanosheet, thus liberating electrons and forming oxygen vacancy. An accumulation layer is therefore formed and the electrical resistance decreased [19].

Namely, adsorption of the target gas molecule and reaction with oxygen have to occur in order to obtain the gas sensing response. Especially, adsorption of the target gas molecule on the surface of the SnO_2 nanosheet is important reaction in order for the oxidation reaction to occur. In the case of the SnO_2 nanosheet, adsorption was unfavourable for the gas molecule which has a methyl group such as CH_4, since

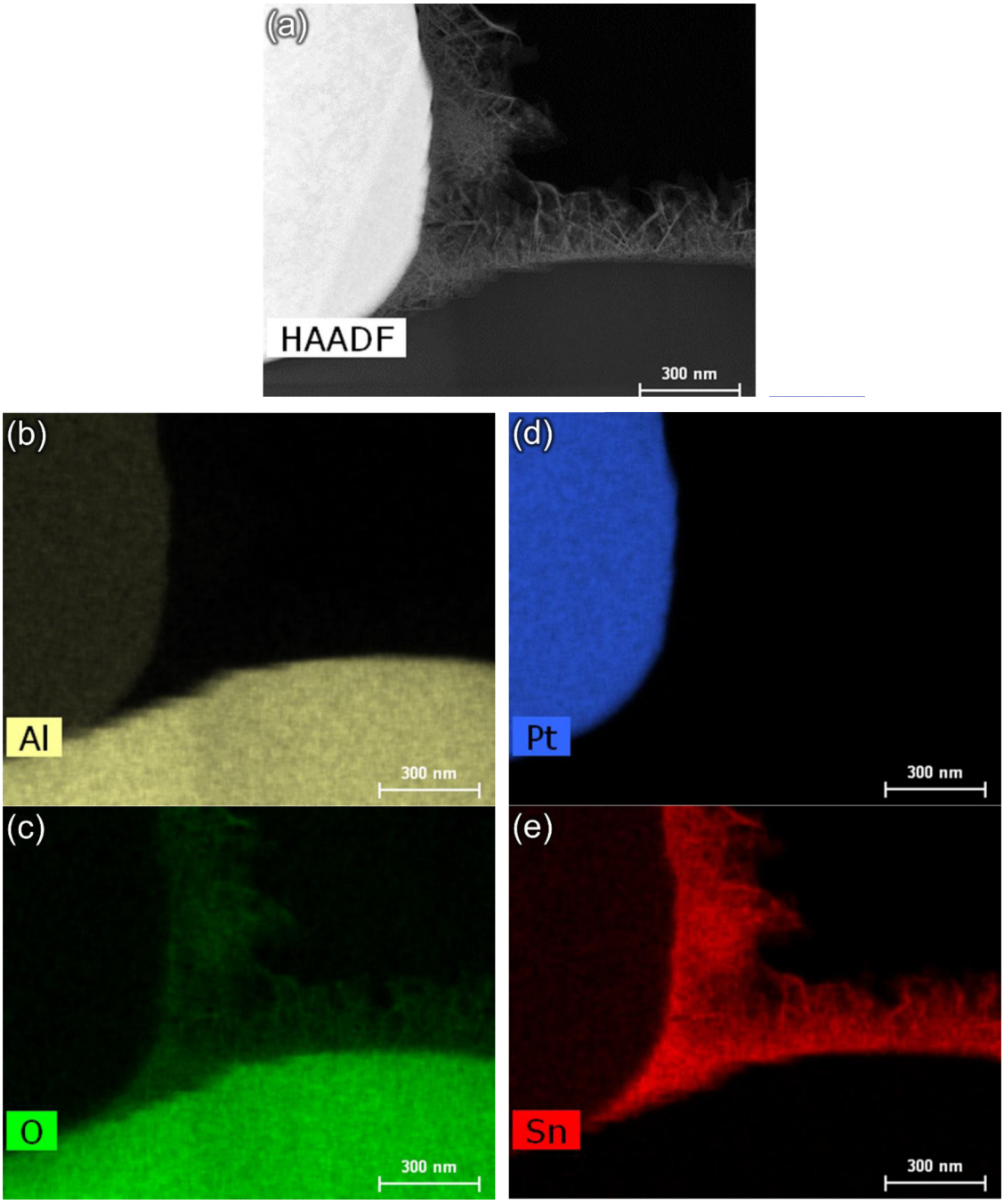

Fig. 7. HAADF and TEM-EDS images of NS; (a) HAADF, (b) Al, (c) O, (d) Pt, and (e) Sn.

the surface has specific exposed crystal facet [19, 20]. Therefore, the sensors both BS and NS exhibited a lower sensing response for CH_4 gas than that for identical concentration of H_2 gas.

Moreover, it is required that target gas molecule react with large amount of oxygen on and in the surface of SnO_2 for high sensing response. Hence, the reason for the high gas sensing selectivity to $C_9H_{18}O$ gas was considered that the space under BS acted as reaction rooms and provide the plenty of time to stay for the reaction (Fig. 11). Additionally, oxidation reaction in the case of the H_2 molecule is as follows [18, 27, 28];

$$H_2 + O^{2-} \rightarrow H_2O \quad (2)$$

H_2 molecule reacted with adsorbed or lattice oxygen (O^{2-}) and H_2O was produced. The reaction is terminated with H_2O desorption. While oxidation reaction in the case of the $C_9H_{18}O$ molecule is as follows [29];

$$C_9H_{18}O + O^{2-} \rightarrow C_9H_{18}O_2 \quad (3)$$

$C_9H_{18}O$ reacted with adsorbed or lattice oxygen and $C_9H_{18}O_2$, nonanoic acid, was produced. The produced $C_9H_{18}O_2$ was desorbed or further react with oxygen until it is completely oxidized, i.e., until CO_2

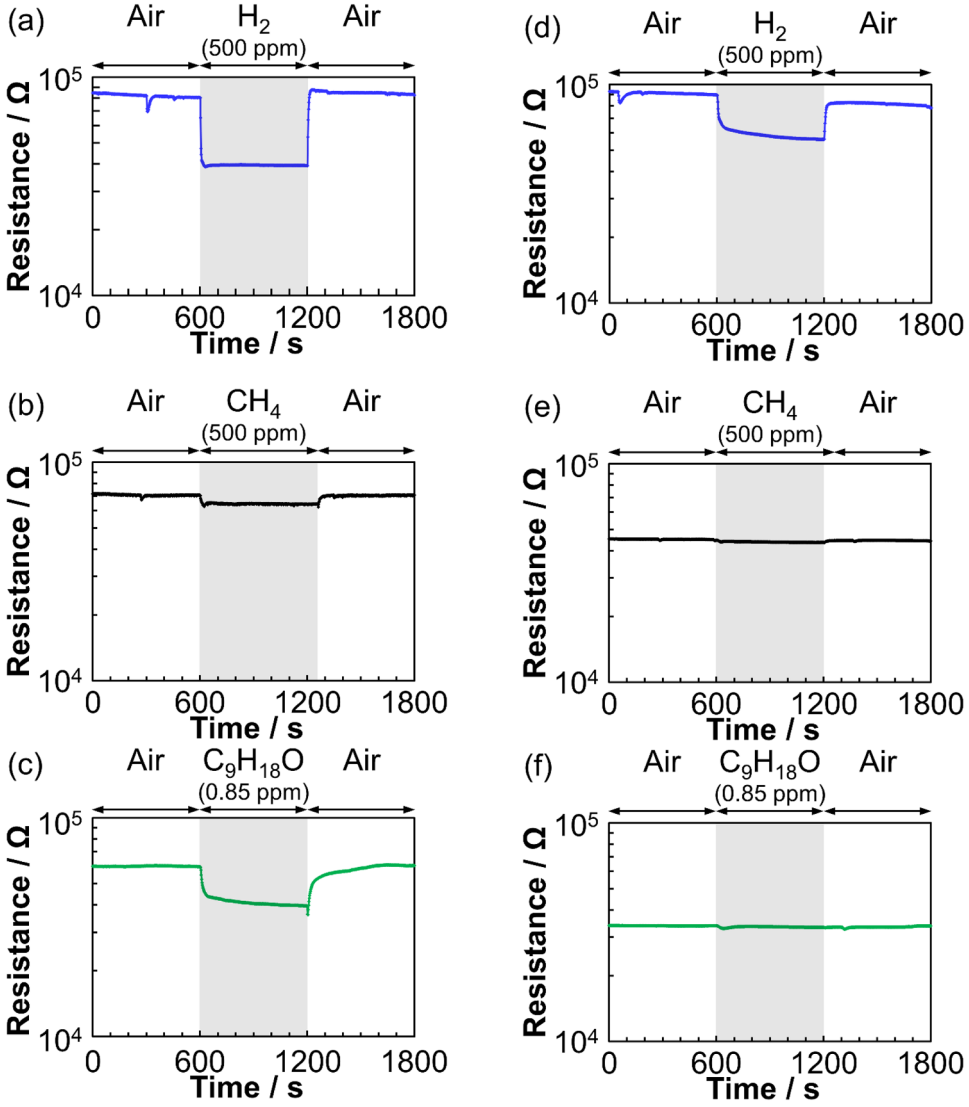

Fig. 8. Resistance variation of BS and NS; (a) BS-500 ppm of H_2, (b) BS-500 ppm of CH_4, (c) BS-0.85 ppm of $C_9H_{18}O$, (d) NS-500 ppm of H_2, (e) NS-500 ppm of CH_4, and (f) NS-0.85 ppm of $C_9H_{18}O$ gases.

and H_2O [29]. The CH_4 molecule produced CH_3 and OH by oxidation reaction as follows [30, 31];

$$CH_4 + O^{2-} \rightarrow CH_3 + OH \quad (4)$$

The produced CH_3 and OH were desorbed or further react with oxygen. The products were released with gas flow after desorption on NS. Whereas re-adsorption of the products on the surface of the SnO_2 nanosheet is favourable reaction in the case of BS, since that has as mentioned reaction room under the thin film. Hence, the sensor signal response of BS considerably increased as compared to that of NS. The result indicates that the sensor signal response for gas molecules which is unfavourable for adsorption and can further react with oxygen by using bridge type structure.

Conclusion

A SnO_2 nanosheet with bridge type structure was fabricated on the Pt interdigitated-electrodes printed SiO_2 substrate via a simple synthesis process. The SnO_2 nanosheet has ca. 150 nm of flat plane and stood perpendicular to the substrate. The SnO_2 nanosheet thin film between Pt interdigitated-electrodes was floated from the substrate. The crystal structure of synthesized SnO_2 defined to tetragonal cassiterite structure of SnO_2. The atomic arrangement corresponds to *d* space of the SnO_2 (101) was observed at the cross-section of the SnO_2 nanosheet via TEM analysis, indicating high degree of crystallinity.

The sensor signal response of the SnO_2 nanosheet thin film with bridge type structure was higher than that of the SnO_2 nanosheet thin film with normal structure. Especially sensor signal response for nonanal gas considerably increased as compared to hydrogen and methane gases even though the concentration of nonanal gas was extremely low. The higher sensing response of the SnO_2 nanosheet thin film with bridge type structure was attributed to introduction of space under thin film which acts as reaction rooms and provide the plenty of time to stay for the reaction.

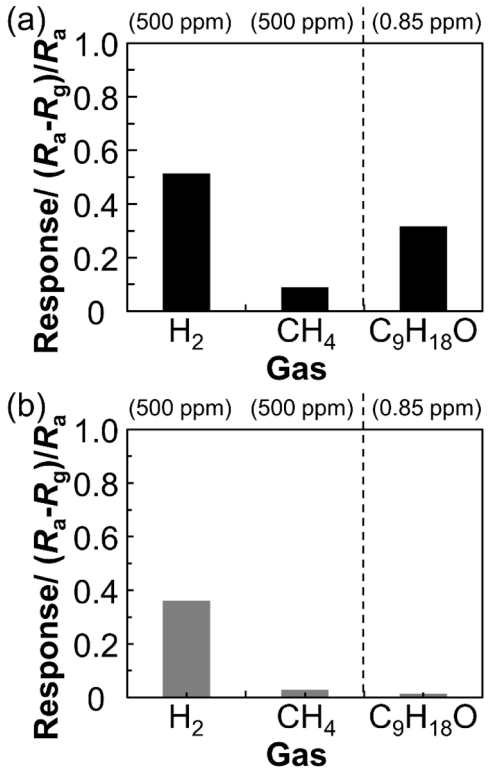

Fig. 9. Sensor signal response of (a) BS and (b) NS for 500 ppm of H_2, 500 ppm of CH_4, and 0.85 ppm of $C_9H_{18}O$ gases.

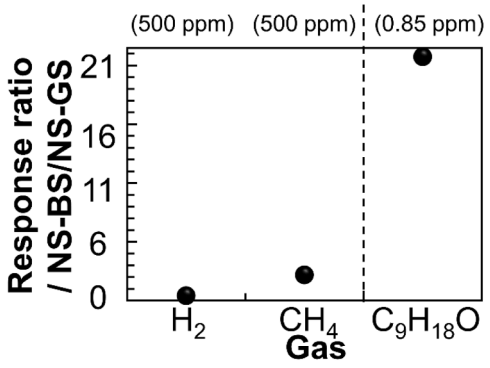

Fig. 10. Sensor response ratio of BS to NS for 500 ppm of H_2, 500 ppm of CH_4, and 0.85 ppm of $C_9H_{18}O$ gases.

CRediT authorship contribution statement

Pil Gyu Choi: Conceptualization, Investigation, Validation, Visualization, Writing - original draft, Writing - review & editing. **Naoto Shirahata:** Funding acquisition, Writing - review & editing. **Yoshitake Masuda:** Conceptualization, Funding acquisition, Project administration, Supervision, Writing - review & editing.

Declaration of Competing Interest

The authors declare that they have no known competing financial interests or personal relationships that could have appeared to influence the work reported in this paper.

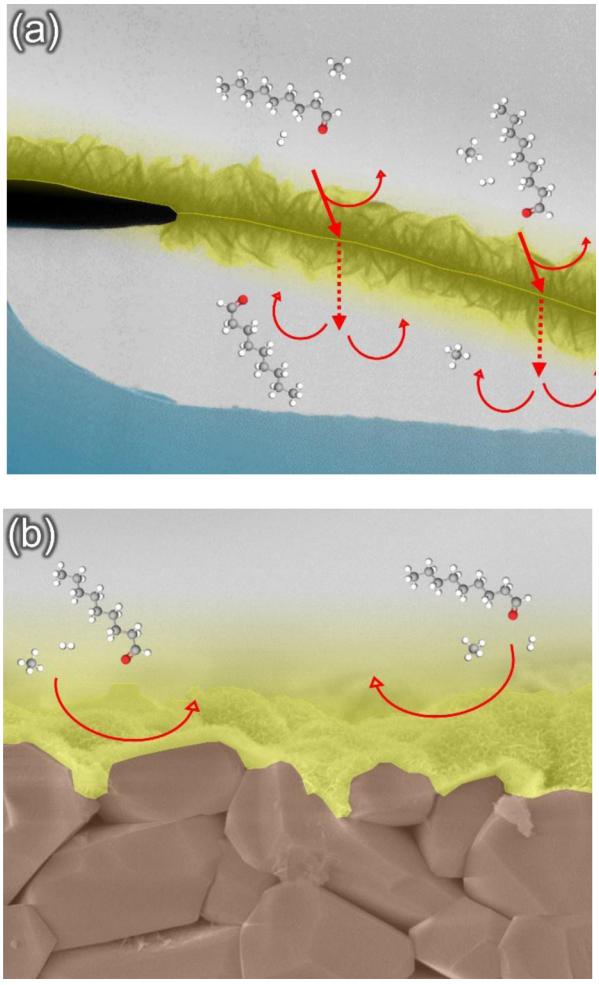

Fig. 11. Schematics illustrations of sensing reaction for (a) BS and (b) NS.

Acknowledgement

This work was supported by the Japan Science and Technology Agency (JST) A-step (JPMJTS1619).

References

[1] S. Haze, Y. Gozu, S. Nakamura, Y. Kohno, K. Sawano, H. Ohta, K. Yamazaki, 2-Nonenal Newly found in human body odor tends to increase with aging, J. Investig. Dermatol. 116 (2001) 520–524.
[2] C. Wongchoosuk, M. Lutz, T. Kerdcharoen, Detection and classification of human body odor using an electronic nose, Sensors 9 (2009) 7234–7249.
[3] P. Fuchs, C. Loeseken, J.K. Schubert, W. Miekisch, Breath gas aldehydes as biomarkers of lung cancer, Int. J. Cancer 126 (2010) 2663–2670.
[4] U.R. Bernier, D.L. Kline, D.R. Barnard, C.E. Schreck, R.A. Yost, Analysis of human skin emanations by gas chromatography/mass spectrometry. 2. identification of volatile compounds that are candidate attractants for the yellow fever mosquito (Aedes aegypti), Anal. Chem. 72 (2000) 747–756.
[5] R.D. Couch, A. Dailey, F. Zaidi, K. Navarro, C.B. Forsyth, E. Mutlu, P.A. Engen, A. Keshavarzian, Alcohol induced alterations to the human fecal VOC metabolome, PLoS ONE 10 (2015) e0119362.
[6] T. Itoh, T. Akamatsu, A. Tsuruta, W. Shin, Selective detection of target volatile organic compounds in contaminated humid air using a sensor array with principal component analysis, Sensors 17 (2017) 1662.
[7] W. Thoren, D. Kohl, G. Heiland, Kinetic studies of the decomposition of CH_3COOH and CH_3COOD on SnO_2 single crystals, Surf. Sci. 162 (1985) 402–410.
[8] L. Wang, S. Wang, Y. Wang, H. Zhang, Y. Kang, W. Huang, Synthesis of hierarchical SnO_2 nanostructures assembled with nanosheets and their improved gas sensing

properties, Sensors Actuators B: Chemical 188 (2013) 85–93.
[9] B. Wang, Y. Wang, Y. Lei, S. Xie, N. Wu, Y. Gou, C. Han, Q. Shi, D. Fang, Vertical SnO_2 nanosheet@sic nanofibers with hierarchical architecture for high-performance gas sensors, J. Mater. Chem. C 4 (2016) 295–304.
[10] Y. Yuan, Y. Wang, M. Wang, J. Liu, C. Pei, B. Liu, H. Zhao, S. Liu, H. Yang, Effect of unsaturated sn atoms on gas-sensing property in hydrogenated SnO_2 nanocrystals and sensing mechanism, Sci. Rep. 7 (2017) 1231.
[11] Z.M. Jarzebski, J.P. Marton, Physical properties of SnO_2 materials: i . preparation and defect structure, J. Electrochem. Soc. 123 (1976) 199C–205C.
[12] M. Batzill, Surface science studies of gas sensing materials: SnO_2, Sensors 6 (2006) 1345.
[13] M. Batzill, U. Diebold, The surface and materials science of tin oxide, Prog. Surf. Sci. 79 (2005) 47–154.
[14] Y. Liu, Y. Jiao, Z. Zhang, F. Qu, A. Umar, X. Wu, Hierarchical SnO_2 nanostructures made of intermingled ultrathin nanosheets for environmental remediation, smart gas sensor, and supercapacitor applications, ACS Appl. Mater. Interfaces 6 (2014) 2174–2184.
[15] P. Sun, Y. Cao, J. Liu, Y. Sun, J. Ma, G. Lu, Dispersive SnO nanosheets: hydrothermal synthesis and gas-sensing properties, Sensors and Actuators B: Chemical 156 (2011) 779–783.
[16] C.S. Moon, H.-.R. Kim, G. Auchterlonie, J. Drennan, J.-.H. Lee, Highly sensitive and fast responding CO sensor using SnO nanosheets, Sensors and Actuators B: Chemical 131 (2008) 556–564.
[17] Y. Masuda, K. Kato, Superhydrophilic SnO nanosheet-assembled film, Thin Solid Films 544 (2013) 567–570.
[18] P.G. Choi, N. Izu, N. Shirahata, Y. Masuda, Fabrication and H_2-Sensing properties of SnO_2 nanosheet gas sensors, ACS Omega 3 (2018) 14592–14596.
[19] P.G. Choi, N. Izu, N. Shirahata, Y. Masuda, Improvement of sensing properties for SnO_2 gas sensor by tuning of exposed crystal face, Sensors Actuators B: Chemical 296 (2019) 126655.
[20] P.G. Choi, N. Izu, N. Shirahata, Y. Masuda, SnO_2 nanosheets for selective alkene gas sensing, ACS Appl. Nano Mater. 2 (2019) 1820–1827.
[21] Y. Masuda, T. Itoh, W. Shin, K. Kato, SnO_2 nanosheet/nanoparticle detector for the sensing of 1-Nonanal gas produced by lung cancer, Sci. Rep. 5 (2015) 10122.
[22] Y. Masuda, T. Ohji, K. Kato, Site-Selective chemical reaction on flexible polymer films for tin oxide nanosheet patterning, Eur. J. Inorg. Chem. (2011) (2011) 2819–2825.
[23] Y. Masuda, T. Ohji, K. Kato, Tin oxide nanosheet assembly for hydrophobic/hydrophilic coating and cancer sensing, ACS Appl. Mater. Interfaces 4 (2012) 1666–1674.
[24] X. Du, Y. Du, S.M. George, CO gas sensing by ultrathin tin oxide films grown by atomic layer deposition using transmission ftir spectroscopy, J. Phys. Chem. A 112 (2008) 9211–9219.
[25] J.N. Zemel, Theoretical description of gas-film interaction on SnO_x, Thin Solid Films 163 (1988) 189–202.
[26] P. Mars, D.W. van Krevelen, Oxidations carried out by means of vanadium oxide catalysts, Chem. Eng. Sci. 3 (1954) 41–59.
[27] M. Shahabuddin, A. Umar, M. Tomar, V. Gupta, Custom designed metal anchored SnO_2 sensor for H_2 detection, Int. J. Hydrogen Energy 42 (2017) 4597–4609.
[28] Y.C. Lee, H. Huang, O.K. Tan, M.S. Tse, Semiconductor gas sensor based on pd-doped sno_2 nanorod thin films, Sensors Actuators B: Chem. 132 (2008) 239–242.
[29] T. Itoh, D. Lee, T. Goto, T. Akamatsu, N. Izu, W. Shin, T. Kasuga, Analysis of recovery time of Pt-, Pd-, and Au-loaded SnO_2 sensor material with nonanal as large-molecular-weight volatile organic compounds, Sensors Mater. 28 (2016) 1165–1178.
[30] A. Das, V. Bonu, A.K. Prasad, D. Panda, S. Dhara, A.K. Tyagi, The role of SnO_2 quantum dots in improved CH_4 sensing at low temperature, J. Mater. Chem. C 2 (2014) 164–171.
[31] I.Y. Pakharukov, I.P. Prosvirin, I.A. Chetyrin, V.I. Bukhtiyarov, V.N. Parmon, In situ xps studies of kinetic hysteresis in methane oxidation over Pt/γ-Al_2O_3 catalysts, Catal. Today 278 (2016) 135–139.